Color Image Processing with Multi-Peak Resonant Tunneling Diodes

WOO HYUNG LEE, Intel Corporation
PINAKI MAZUMDER, University of Michigan at Ann Arbor

18

The article introduces a novel approach to color image processing that utilizes multi-peak resonant tunneling diodes for encoding color information in quantized states of the diodes. The Multi-Peak Resonant Tunneling Diodes (MPRTDs) are organized as a two-dimensional array of vertical pillars which are locally connected by programmable passive and active elements with a view to realizing a wide variety of color image processing functions such as quantization, color extraction, image smoothing, edge detection, and line detection. In order to process color information in the input images, two different methods for color representation schemes have been used: one using color mapping and the other using direct RGB representation. Finally, the article uses HSPICE simulation methods for the nestlist of the proposed RTD-based nanoarchitecture in order to verify a candidate of image functions by using the afore-mentioned representation methods.

Categories and Subject Descriptors: C.5.4 [**Computer System Implementation**]: VSLI Systems

General Terms: Design

Additional Key Words and Phrases: VLSI, quantization, color extraction, color image processing, resonant-tunneling diode(s), cellular neural network

ACM Reference Format:
Lee, W. H. and Mazumder, P. 2013. Color image processing with multi-peak resonant tunneling diodes. ACM J. Emerg. Technol. Comput. Syst. 9, 3, Article 18 (September 2013), 20 pages.
DOI: http://dx.doi.org/10.1145/2503128

1. INTRODUCTION

Since 1987 when the Cellular Neural Networks (CNN) paradigm of massively parallel computing through local interactions between an ensemble of simple processing elements capable of aggregating the weighted analog stimuli from their neighboring processors and generating digital outputs was first developed by Chua and Yang [1988; Hänggi and Chua 2001], it has rapidly morphed into a general-purpose powerful backend hardware substrate to accelerate several classes of nonnumber crunching computations much faster than conventional digital computers can perform within the constraint of energy budget as well as Silicon real estate. Several types of two- and multidimensional spatial data processing used in color image analysis [Wang et al. 1998], video motion detection [Lee and Mazumder 2008], DNA microarray pattern classification [Arena et al. 2002], real-time brain waves study in epileptic episodes [Tetzlaff et al. 1999], and in many other real-world applications have been successfully demonstrated by both analog and digital implementations of the CNN array embedded within a single VLSI chip. However, ultimately heat dissipation and Silicon areas of conventional

This work is supported by the National Science Foundation.
Authors' addresses: W. H. Lee, Intel Corporation, 2200 Mission College Boulevard, Santa Clara, CA 95054; P. Mazumder (corresponding author), Electrical Engineering and Computer Science Department, University of Michigan at Ann Arbor, 1301 Beal Avenue, Ann Arbor, MI 48109; email: mazum@eecs.umich.edu.

DOI: http://dx.doi.org/10.1145/2503128

CNN cells limit the size of CMOS-based CNN arrays to 256×256 processing elements or so, thereby severely limiting the resolution of the input and the output data. The goal of this article is to describe the design of a new quantum tunneling device (called Multi-Peak Resonant Tunneling Diode, MPRTD) based on a nonlinear dynamical system capable of performing various types of color image processing tasks with higher precision. Though nanoscale MPRDT-based neurons (processing elements) along with their programmable synapses comprising both passive and active devices strikingly differ from CMOS-based analog and digital CNNs, the overall behavior of the nonlinear system has been shown in this article to mimic the CN paradigm of computation.

The Resonant Tunneling Diode (RTD) was invented by Chang, Esaki, and Tsu [Chang et al. 1974] in the early seventies by demonstrating that when a bias voltage is applied across its two terminals, the *I-V* characteristic of the RTD has a folded-back shape owing to the tunneling through the mesoscale double-barrier quantum well of the RTD. This Negative Differential Resistance (NDR) characteristic of the RTD has been cleverly exploited by a number of researchers to design several high-speed and high-density integrated circuits [Mazumder et al. 1998; Seabaugh and Mazumder 1999; Haddad and Mazumder 1997; Ding and Mazumder 2004] as well as utilized to build CNNs with improved speed and integration density [Hänggi and Chua 2001]. Vertically integrated RTDs have subpico-second switching speed as opposed to planar and sluggish PMOS and NMOS devices, thereby enabling the RTD-based digital and CNN systems to have superior power-delay performance to their CMOS counterparts. To show the advantages of RTDs in CNN architectures, Hänggi and Chua [2001] incorporated RTDs in CNN processing elements and implemented monochromatic image processing by using the self-latching bistable (1-bit storage) property of the RTD.

However, in order to perform color image processing, the simple RTD configuration of [Hänggi and Chua 2001] is not adequate since color images need more than one bit per pixel. In this article, we discuss a new type of two-dimensional array consisting of the MPRTDs and programmable synapses that may consist of resistive, capacitive, and active devices. Since MPRTDs are fabricated by vertically stacking double-barrier (one-peak) RTDs, the resulting three-dimensional architecture requires very small Silicon area. Waho et al. [1998] implemented multiple thresholds and outputs using the planar RTDs configured into MOBILE (Monostable to bistable transition logic elements) mode. In this article, we have realized color image processing by implementing multiple output levels with vertically stacked RTDs grown under the metallic islands as shown in Figure 1. To demonstrate simulation results, we used a piecewise continuous model of an eight-peak RTD with 9 stable states which was originally fabricated at Texas Instruments by stacking serially eight pseudomorphic ALAs/In0.53Ga0.47As/InAs RTDs and the existence of 9 states was experimentally verified by Seabaugh et al. [1992]. To exploit the nine stable states for color image processing, we introduce two different methods for the color representation: color mapping and RGB encoding. While the first method uses a color map to index the color value, the latter method uses three cells to represent RGB (Red, Green, and Blue) colors for a single pixel. Using the color depiction methods and characteristics of the multi-peak RTDs, we describe several color image processing functions such as quantization, smoothing, and color extraction.

2. THE MULTI-PEAK RTD-BASED COLOR IMAGE PROCESSOR

Silicon-based Resonant Tunneling Diodes (RTDs) are touted as a strong candidate to augment the performance of conventional CMOS circuits by largely replacing bulky and sluggish PMOS transistors generally used in the pull-up network. The *I-V* device characteristics of the RTD comprise three distinct regions, namely, two Positive Differential Resistance (PDR) regions and one intervening Negative Differential Resistance (NDR) region, as shown in Figure 1(top). The resulting nonmonotonic tunneling

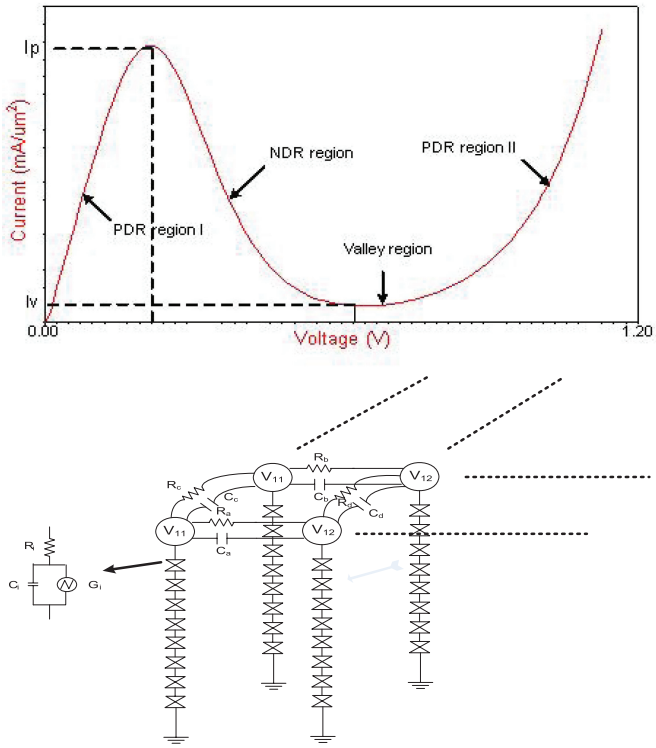

Fig. 1. I-V characteristic of a resonant tunneling diode (top) and side view and top view of the multi-peak RTD-based image processor (bottom).

characteristics of the RTD can be cleverly exploited in key circuit nodes to significantly improve the device performance in terms of power and delay, thereby yielding low power-delay product in comparison to other forms of CMOS circuits [Roychowdhury et al. 1996; Karahaliloglu and Balkir 2002; Lee and Mazumder 2008]. A definite advantage of RTD-based circuits is that they are generally more processvariation tolerant since the operation of the RTD remains unaffected as long as its peak current I_P is higher than its valley current I_V.

RTD-based image processors published in the literature utilized the bistable state of the resonant tunneling diode [Roychowdhury et al. 1996; Karahaliloglu and Balkir 2002; Karahaliloglu et al. 2003] to decide the output image and processing methods. By using parallel processing and small intrinsic capacitance, fast image processing is possible with this structure. The disadvantage is that it is impossible to present various functions, to generate color images, and to process those color images because three stable states are required to display color information. Multiple stable states are essential to represent the color information due to the various color values. Each RTD can be modeled as the R-C-, and voltage-controlled current source in the circuit simulation. Multi-peak RTDs are built by stacking single-peak RTDs to obtain 9 states in this article, though in practice any number of states can be realized as long as the process of RTD stacking is possible. As we discussed before, we used 9 states because it was proven RTD stats by experimental results [Seabaugh et al. 1992]. If the process evolves more and allows more stacking the RTDs, then we can use more stable states for our color image processor.

In Figure 1, the interconnection between two multi-peak RTDs is implemented with the RC models. This RC model changes based on the image function that the processor realizes. In the CNN perspective, the changes of the RC model parameters correspond to the change of the templates in the CNNs. For implementation of the conductance network, Roychowdhury et al. [1996] showed the feasibility of implementation and initial guidance for a more complex conductance network.

The I-V characteristics of the multi-peak RTD in the vertical direction can be simply piecewise linearly modeled as shown in Figure 2(a). Since the eight-peak RTD is used, nine stable states exist when using a constant current source that delivers current in the range between the lowest peak current and the highest valley current. However, the I-V curve of the experimental data shows a DC shift as shown in Figure 2(b). To be valid in functionality, the lowest peak should be higher than the highest valley. These peak or valley values also change based on the size of the metallic islands. Since the size of RTDs varies depending on the process variation, we need to consider the shift of I-V curve to up and down in the direction. Based on the experimental result from Seabaugh et al. [1992], if the size deviation of the metallic islands is 67% to bigger size or 33% to smaller size, the functionality is guaranteed. The process variation also affects the power dissipation and speed. However, the overall speed and power dissipation are not much changed if we assume randomly distributed inputs. The worst pixel speed is degraded around 30 ps from Eq. (9) and the power dissipation of the worst pixel is increased around 0.2 nW from Eq. (14). The overall speed and power dissipation is more dependent on the initial value of output and templates as shown in Figure 5, Figure 8, and Figure 13. In the case of the smoothing function, the stabilization time and power dissipation is proportional to the difference between the initial color and the smoothed output color. The discrepancy between the initial color and the background color affects the stabilization time and power dissipation proportionally for the color extraction function.

The standard CNN state equation can be written as [Chua and Yang 1988; Karahaliloglu and Balkir 2002; Lee and Mazumder 2008; Hänggi and Chua 2001]

$$\frac{dx_{ij}}{dt} = -x_{ij} + \sum_{k,1\in N_{i,j}} (a_{k-i,l-j} f(x_{kl}) + b_{k-i,l-j} u_{kl}) + I_{ij}, \tag{1}$$

where $X_{ij} \in R$, $f(X_{ij}) \in R$, $u_{kl} \in R$, and $I_{ij} \in R$ denote the state, output, input, and threshold. *a(i,j;k,l)* and *b(i,j;k,l)* are called the feedback and the feed-forward operators or templates, respectively. Considering the network connection between cells and neglecting the feed-forward effect, Eq. (1) can be transformed into Eq. (2) that follows which will be used for quantization, smoothing, and color extraction.

$$\frac{cdv_{ij}}{dt} = -J(v_{ij} + \sum_{k,l\in N_{i,j}} (a_{k-i,l-j} v_{kl}) + I_{ij} \tag{2}$$

Here the template

$$a = \begin{bmatrix} 0 & q & 0 \\ q & -4q & q \\ 0 & q & 0 \end{bmatrix}$$

I_{ij} is the driving current, and C is the contact capacitance of each RTD.

In the cases of quantization and smoothing function, the template for feedback is represented as a_{ij} in Eq. (2). The template for the quantization function and smoothing function is decided by the conduction from the neighboring cells to the target cell. In the preceding example, there is a target cell that has connections with four

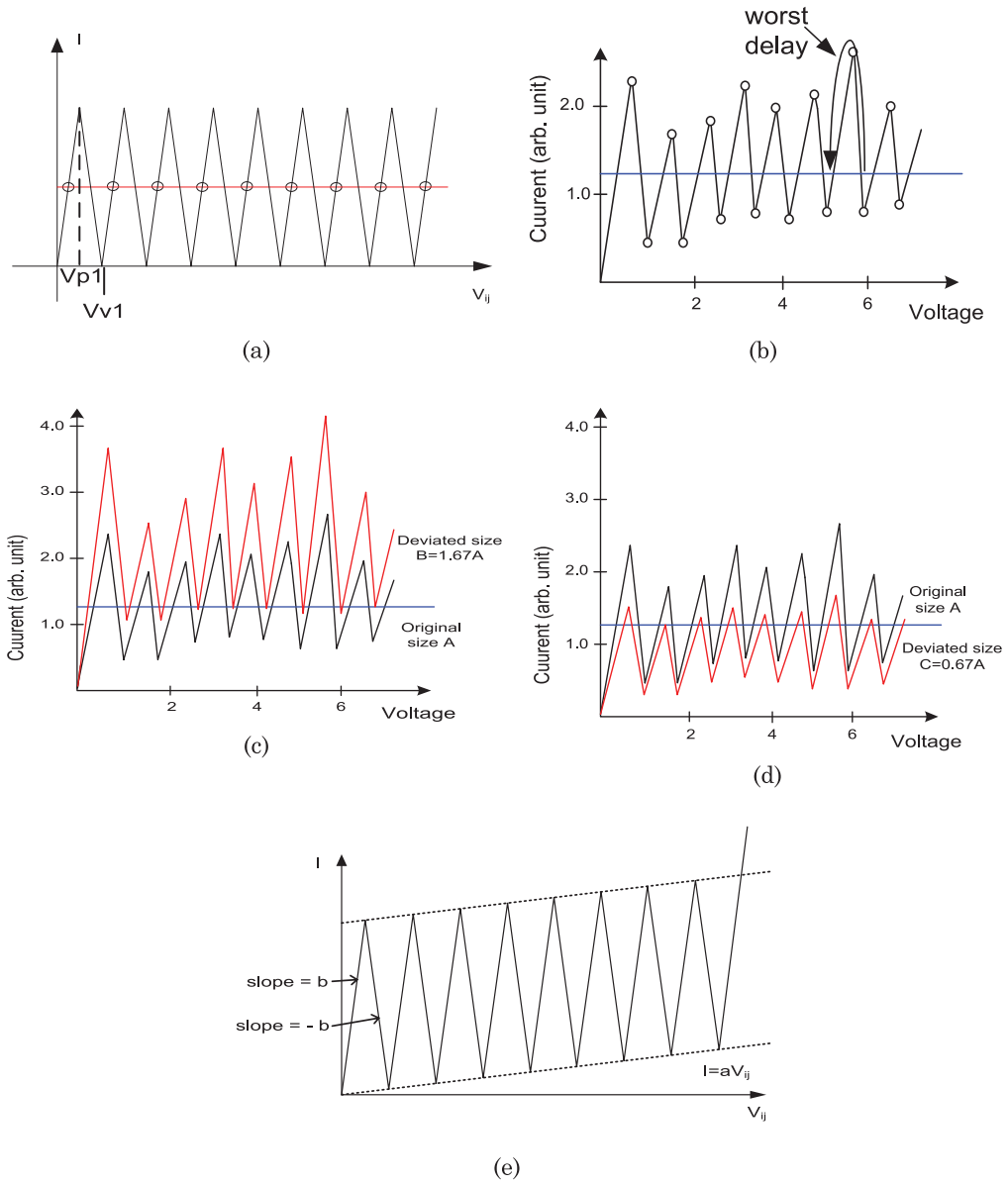

Fig. 2. Simplified piecewise-linear model of I-V characteristics for an eight-peak RTD in the vertical direction (a), piecewise-linear model based on experimental data (b), maximum size deviation for valid functionality (c), minimum size deviation for valid functionality (d) and piecewise-linear model with a linear DC shift (e).

neighboring cells with q conduction value. The center cell has −4q conduction value that means that it reversely dissipates the incoming current. By the value of q in the template, the quantization function or smoothing function is decided. The quantization and smoothing function are realized with resistive network connection with the defined neighboring cells in the template. So, the current flows from the four neighboring cells to the center cell or reverse direction. The center cell circulates the received currents through itself to satisfy the KCL. Also, this current flow depends on the outputs of the

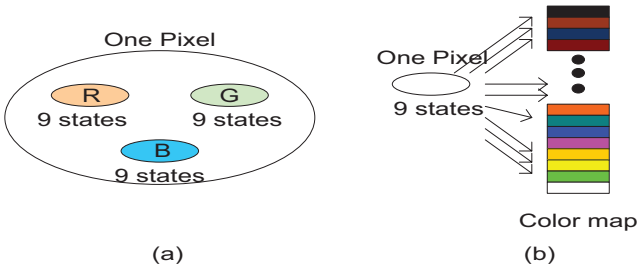

Fig. 3. The color representation methods with metallic islands on the eight-peak RTDs. (a) RGB value method and (b) color map method.

neighboring cells. Hence, the template a_{ij} is represented as a matrix that has q in the left, right, up, and down current flow and -4q for the center cell. The value of q is a conductance value in a real number that changes depending on the image functions.

The I-V curves of Figure 2(a) and (e) can be represented as Eq. (3) and Eq. (4), respectively. Even if Eq. (4) demonstrates a more realistic curve form based on the experimental data, Eq. (3) is chosen for a model for the eight-peak RTD since the functionality is not affected with simple implementation and the overall processing time changes less than 30 ps (5%) from Eq. (9) and Figure 5. This is because the initial voltage and the templates of each cell more affects the processing time than the eight-peak RTD models.

$$J(V_{ij}) = \begin{cases} \alpha(V_{ij}) \, if \; 0 < V_{ij} \leq V_{p1} \\ \alpha(|V_{ij} - n \cdot V_{p1}|) \, if \; (2n-1)V_{p1} < V_{ij} \leq (2n+1)V_{p1} \end{cases} \tag{3}$$

$$J(V_{ij}) = \begin{cases} b((V_{ij} - n) \cdot k, & 0 < V_{ij} \leq \dfrac{nc_1}{2b} \\ -b((V_{ij} - n) \cdot k) + c_1, & \dfrac{nc_1}{2b} < V_{ij} \leq \dfrac{nc_1}{a+b} \end{cases} \tag{4}$$

Here n is an integer from 1 to 8 and k is the real number of the shift amount.

3. COLOR REPRESENTATION METHOD

As shown in Figure 2(a) and (b) and Eq. (3), an eight-peak resonant tunneling diode has nine stable states. The nine states can be used to indicate color values that can be used for processing the color images.

Two methods are suggested to store color images using the array of the eight-peak RTDs. One method is to match the voltages of the array of the eight-peak RTDs to color index values. In this method, each index value designates each color in the color map as shown in Figure 3(b). This method, called the color map method, is used for color images that have color maps.

However, there is a limitation of the color number in this method. The maximum number of colors to represent is 9 because the eight-peak RTD has nine stable states. Despite this drawback, the color map method is easier to perform in fabrication than the other method. The second method uses three metallic islands to represent one pixel, and each metallic island corresponds to the Red, Green, and Blue (RGB) colors. The voltage value of the metallic island indicates the intensity of the RGB color. Since each metallic island can express the 9 different intensities, a total of 729 colors can be represented, and the number of colors can be extended by increasing the number

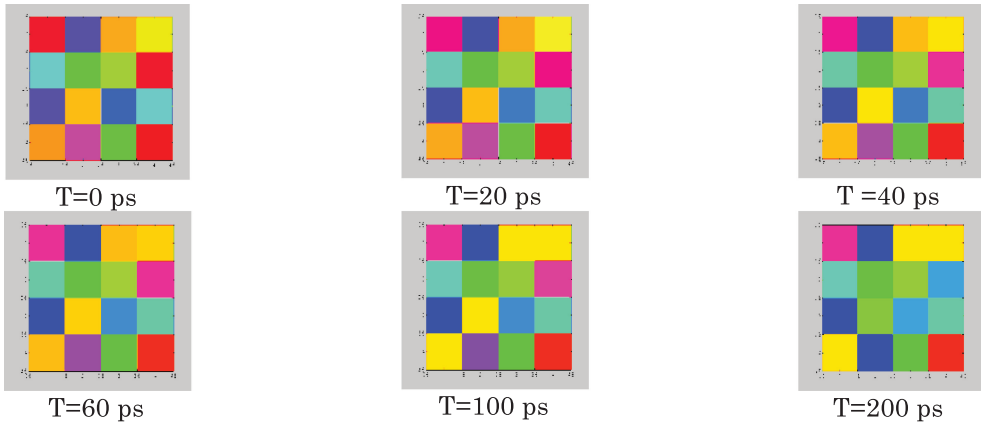

Fig. 4. Transient representation of 4 × 4 color image quantization from 0 ps to 200 ps.

of metallic islands per pixel. This method is called RGB color method as shown in Figure 3(a), and is used to process bitmap images.

The multiple quantization levels can also be used to provide gray scale to images. If we assume three multi-peak RTDs represent one gray scale, a total of 729 gray levels can be represented for images. A fine resolution can be achievable in the gray images due to the previous fact. This will be useful when we implement the smooth function which requires polishing the edges of gray levels in the neighboring pixels.

4. COLOR QUANTIZATION

4.1. Implementation and Results

Using the discrete stable states of the multi-peak RTDs, the color quantization is implemented. Figure 4 represents the changes of colors of a 4 × 4 pixel image. This change of the color image arises from the I-V characteristics of the multi-peak RTDs. From the initial color value, the quantized value is obtained by the minimum Euclidean distance. From Eq. (3), the quantized color value can be obtained as a function of I_{ij}.

$$J(v_{ij}) = I_{ij} \tag{5}$$

$$v_{ijk} = J^{-1}(I_{ij}) \tag{6}$$

Here v_{ijk} is the solution of Eq. (3) and $k = 1, 2, \ldots, 9$, where 1 corresponds to the lowest value of the solution and 9 corresponds to the highest value of the solution in Figure 3. If we assume that the input image value is u_{ij}, the minimum Euclidean distance can be derived as follows.

$$Dist_{\min} = \min_{k\,=\,1,\,..,\,9} \left(|u_{ij} - v_{ijk}|\right) \tag{7}$$

The solution of Eq. (3) which has the minimum Euclidean distance is the quantization value. The change from the unstable state to the stable state is depicted in Figure 5. In Figure 5, the time to get to the final stable state is confirmed by monitoring the tracks of colors in the images. As shown in the HSPICE simulation results, the color values are stabilized after 200 ps. The images representing the HSPICE simulation results show the same characteristics. Based on the simulation, the minimum connection resistance between the metallic islands is 250 MΩ to implement the quantization function.

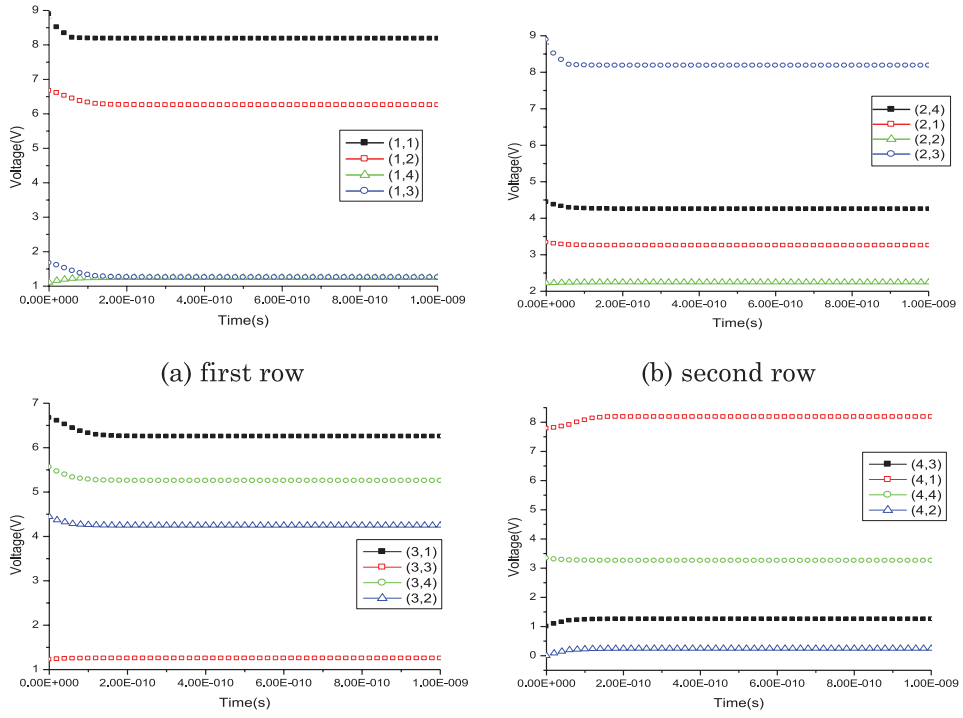

(a) first row (b) second row

(c) third row (d) fourth row

Fig. 5. HSPICE simulation results divided into rows with time from 0 ns to 1 ns.

The feedback template and feed-forward template for the quantization function are represented as

$$a = \begin{pmatrix} 0 & k & 0 \\ k & -4k & k \\ 0 & k & 0 \end{pmatrix}, \quad b = \begin{pmatrix} 0 & 0 & 0 \\ 0 & 0 & 0 \\ 0 & 0 & 0 \end{pmatrix},$$

where k is the conductance between the neighboring cells and center cell. The typical value for k is greater than 0.01 μmho. External current value should be chosen to be between the lowest peak and the highest valley in the I-V curve.

4.2. Settling Time Analysis

The settling time of the array of the multi-peak RTD structure is defined as the time needed to reach the stable state from the initial condition value. The stabilization time is determined by the slowest cell in the CNN. In Eq. (2), if we assume the initial voltage is v_0, then the solution of the first-order differential equation is given as

$$v(t) = \left[v_0 - \left(\frac{I_{ij}}{a + \sum_{k,l \in N_{i,j}} a_{k-i,l-j}} \right) \right] e^{-t(a + \sum_{k,l \in N_{i,j}} a_{k-i,l-j})/c} + \frac{I_{ij}}{a + \sum_{k,l \in N_{i,j}} a_{k-i,l-j}} \tag{8}$$

From Eq. (8), the output of the center cell is changed when a set of neighboring cells is interconnected by any template. If the template is changed, a vector $a_{k-i,l-j}$ is also changed. The changed vector affects the conductance between the neighboring cells

Table I. Comparison of the Stabilization Time among the Image Processing Functions

	Worst	Best	Avg.
Quantization	120 ps	50 ps	83 ps
Smoothing	0.05 ns	0.7 ns	0.35 ns
Color extraction	0.05 ns	1.3 ns	0.7 ns

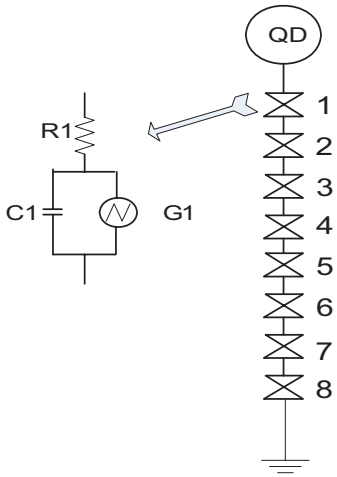

Fig. 6. Equivalent circuit model of the multi-peak RTDs for color quantization.

and the center cell from Eq. (8), and the output of the center cell is stabilized when there is no change in the current flow which is changed by the template and the outputs of the neighboring cells.

The current from the feedback operator in the quantization function is negligible, so Eq. (8) can be approximated as

$$v(t) = \left(v_0 - \frac{I_{ij}}{a}\right) e^{-ta/c} + \frac{I_{ij}}{a}. \tag{9}$$

From Eq. (9), the difference between the initial voltage and the quantized voltage is proportional to the stabilization time. The stabilization time is maximal in the initial voltages where the red line meets the negative slope of the I-V curve as in Figure 2.

In Table I, the stabilization time according to image processing functions is demonstrated. The stabilization time depends on the image processing function. This is attributed to the change of the template between the image processing functions. The changed template (α) in Eq. (9) affects the output $v(t)$ leading to the deviation of stabilization time.

4.3. Power Consumption Analysis

The information on the power consumption of the multi-peak RTDs is needed to determine whether the array of the multi-peak RTDs is energy efficient. For quantization, the equivalent circuit model is shown in Figure 6, where we assume the current flows vertically from the metallic islands to the substrate. The I-V characteristic of the G1 is defined by the multi-peak resonant tunneling diode. To use the negative differential resistance characteristic of the device, we need to flow current which is between the peak value and the valley value in the I-V curve of the device. We also assume the current between the metallic islands for quantization is negligible. In Figure 6, each

one-peak RTD can be modeled with a resistance serially connected to a capacitor and nonlinear voltage controlled current source with a parallel connection. The supplied input energy stored on the capacitor is expressed by

$$\begin{aligned} E_{v0} &= \int_0^\infty i_0(t) \cdot v_0 dt \\ &= v_0 \int_0^\infty C_{total} \frac{dv_0}{dt} dt \\ &= C_{total} v_0 \int_0^\infty dv_0 \\ &= C_{total} v_0^2, \end{aligned} \tag{10}$$

where C_{total} is the sum of the serially connected capacitances. Considering the external current source, the energy supplied to the quantum dot equals

$$\begin{aligned} E_{total} &= E_{v0} + E_{ext} \\ &= C_{total} v_0^2 + I^2 R_{total}, \end{aligned} \tag{11}$$

where R_{total} is the summation of the serially connected resistances in the vertical direction. The energy of the capacitor after the quantization is given as

$$\begin{aligned} E_{Voutput} &= \int_0^\infty i_{Vinput}(t) \cdot v_{output}(t) dt \\ &= \int_0^\infty C_{total} \frac{dV_{output}}{dt} \cdot v_{output}(t) dt \\ &= \frac{C_{total} v_{output}^2(t)}{2}. \end{aligned} \tag{12}$$

In Eq. (11), the output voltage changes with time in Eq. (8). From Eq. (8), the energy change with time is expressed by the following equation.

$$E_{Voutput} = \frac{C_{total}}{2} \left[\left(v_0 - \frac{I}{a} \right) e^{-ta/c} + \frac{I}{a} \right]^2 \tag{13}$$

Therefore, the energy consumption after quantization is given as

$$\begin{aligned} E_{diss} &= E_{total} - E_{Voutput} \\ &= C_{total} v_0^2 + I^2 R_{total} \\ &\quad - \frac{C_{total}}{2} \left[\left(v_0 - \frac{I}{a} \right) e^{-ta/c} + \frac{I}{a} \right]^2. \end{aligned} \tag{14}$$

5. SMOOTHING FUNCTION

5.1. Implementation and Results

As shown in Figure 7, the changes in the pixel values due to the multi-peak RTD and resistance between metallic islands are depicted. These color changes arise from the current change in each metallic island that is connected with resistors. In this simulation, we chose 50 MΩ for the connection resistors. As shown in the Figure 7, the colors in the neighboring positions change such that the color values between neighbor cells are similar. This phenomenon provides a way of detecting similarity of the detected colors nearby. The color similarity can be detected when the similar color pixels are merged to the same color in the long run.

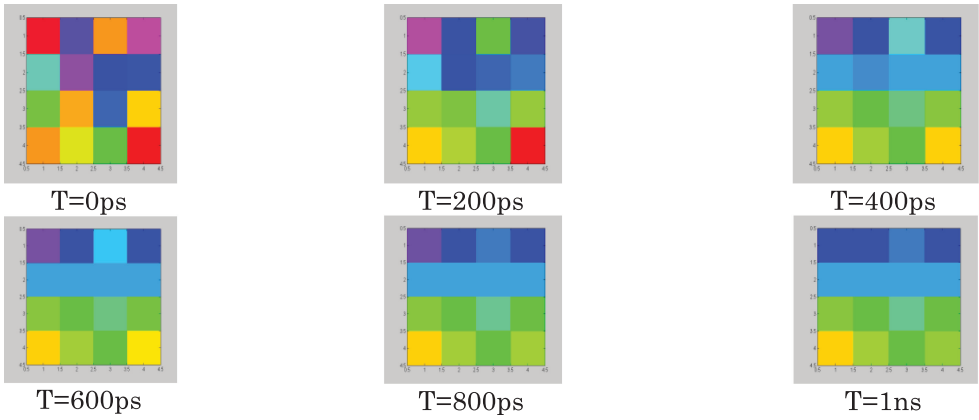

Fig. 7. Transient representation of a 4 × 4 color image for the smoothing function from 0 ps to 200 ps.

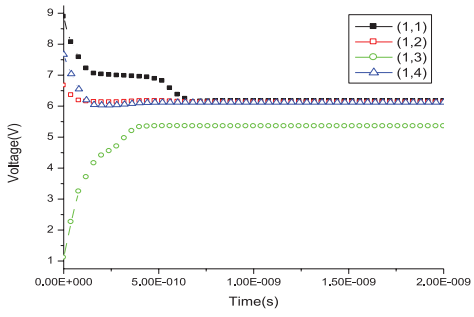

(a) first row

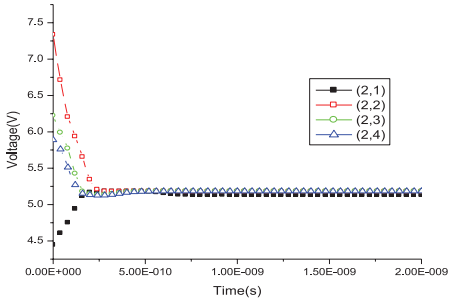

(b) second row

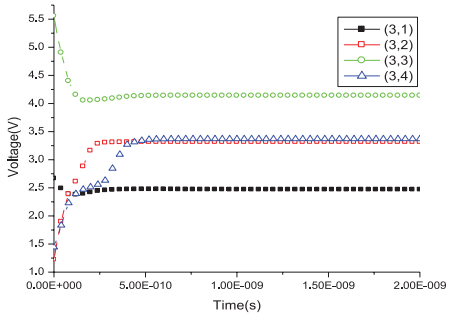

(c) third row

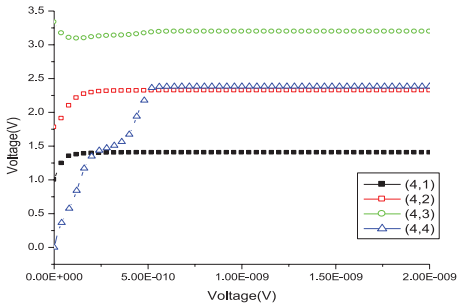

(d) fourth row

Fig. 8. HSPICE results divided into rows with time from 0 to 2 ns.

Also, the traces of the image color that change with time arise from the negative differential resistance that is one of the characteristics of the resonant tunneling diodes. Therefore, the simulation results reflect both the effects of resistances that connect the nearest-neighbor cells and the negative differential resistance characteristic. In Figure 8, the change in the color images shows that the colors of the first row and the

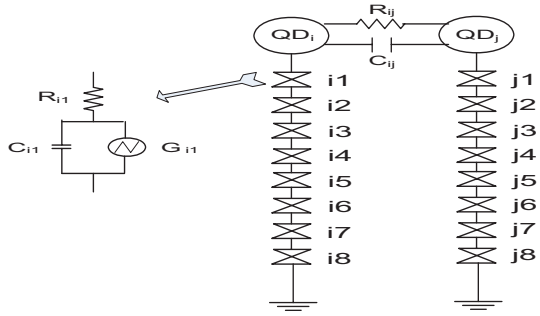

Fig. 9. Equivalent circuit model of the array of the multi-peak RTD structure for the smoothing function.

second row are quite different from those of the other rows, which are also shown in the simulation results as the affinity of colors. In addition, the color value change by the neighboring cells can be applied to the noise removal of an image.

The feedback template and feed-forward template for the smoothing function are represented as

$$a = \begin{pmatrix} 0 & l & 0 \\ l & -4l & l \\ 0 & l & 0 \end{pmatrix}, \quad b = \begin{pmatrix} 0 & 0 & 0 \\ 0 & 0 & 0 \\ 0 & 0 & 0 \end{pmatrix},$$

where l is conductance between the neighboring cells and center cell. The typical value for l is between 0.04 and 0.02 μmho. Then, the output changes based on Eq. (8).

5.2. Stabilization Time

As shown in Figure 8, the settling time of the smoothing function is longer than that of the quantization function. This difference is attributed to the feedback operation in Eqs. (2) and (8). In Eq. (8), the feedback operation term works as a function increasing the settling time. After the system is settled, the feedback operation term becomes zero. Hence, Eq. (9) describes the smoothing function after settling.

5.3. Power Consumption Analysis

To analyze the smoothing function, we simplify the array of the multi-peak RTD structure as two cells as shown in Figure 9. We then expand the two cells to an $N \times N$ array. If the voltages of the two cells are equal, the power consumption will be the same as that in the quantization function. When the voltages of the two cells are different and $V_{QDj} > V_{QDi}$, the supplied input energy is expressed by the following equation.

$$\begin{aligned} E_{v0} &= \int_0^\infty i_0(t) \cdot (v_{0i} + v_{0j}) dt \\ &= v_{0i} \int_0^\infty C_t \frac{dv_{0i}}{dt} dt \\ &\quad + v_{0j} \int_0^\infty C_t \frac{dv_{0j}}{dt} dt \\ &= C_t v_{0i} \int_0^\infty \mathrm{d}v_{0i} + C_t v_{0j} \int_0^\infty dv_{0j} \\ &= C_t \left(v_{0_i}^2 + v_{0_j}^2 \right) \end{aligned} \tag{15}$$

Here C_t is the sum of the capacitances surrounding the cells. Including the energy from the external current source, the total energy supplied is given as

$$\begin{aligned} E_{total} &= E_{v_{oi}} + E_{v_{oj}} + 2E_{ext} \\ &= C_t v_{0i}^2 + C_t v_{0j}^2 + 2I_{ij}R_{total}. \end{aligned} \tag{16}$$

Considering current from QD_i to QD_j, the energy after the smoothing function is expressed by the following equation.

$$\begin{aligned} E_{Voutput} & \int_0^\infty i_{QDi}(t) \cdot v_{QDi}(t)dt \\ &+ \int_0^\infty i_{QDj}(t) \cdot v_{QDj}(t)dt \\ &= \int_0^\infty C_t \frac{dV_{QDi}}{dt} \cdot v_{QDi}(t)dt \\ &+ \int_0^\infty C_t \frac{dV_{QDj}}{dt} \cdot v_{QDj}(t)dt \\ &= \frac{C_t v_{QDi}^2(t)}{2} + \frac{C_t v_{QDj}^2(t)}{2} \end{aligned} \tag{17}$$

$$\begin{aligned} v_{QDi}(t) &= \left[v_0 - \left(\frac{I_{ij}}{a - (1/R_{ij})}\right)\right] e^{-t(a-(1/R_{ij}))/C} \\ &+ \frac{I_{ij}}{a - \frac{1}{R_{ij}}} \end{aligned} \tag{18}$$

$$\begin{aligned} v_{QDj}(t) &= \left[v_0 - \left(\frac{I_{ij}}{a + (1/R_{ij})}\right)\right] e^{-t(a+(1/R_{ij}))/C} \\ &+ \frac{I_{ij}}{a + \frac{1}{R_{ij}}} \end{aligned} \tag{19}$$

The total energy consumption used for the smoothing function is given as

$$\begin{aligned} E_{diss} &= E_{total} - E_{Voutput} \\ &= C_t\left(v_{0i}^2 + v_{0j}^2\right) + 2I_{ij}^2 R_{total} \\ &\quad - \frac{C_t}{2}\left(v_{QD_i}^2(t) + v_{QD_j}^2(t)\right). \end{aligned} \tag{20}$$

If we expand the two dots to an $N \times N$ array, the total energy consumption is modified as follows.

$$\begin{aligned} E_{diss} &= E_{total} - E_{Voutput} \\ &= C_t \sum_{n=1}^{N^2} v_{0n}^2 + 4N^2 \cdot I_{ij}^2 R_{total} - \frac{C_t}{2} \sum_{n=1}^{N^2} V_{QDn}^2(t) \end{aligned} \tag{21}$$

6. COLOR EXTRACTION

We need three cells each pixel output for the color extraction function. Nine cells are required if we represent the color image with the RGB method. The relationship

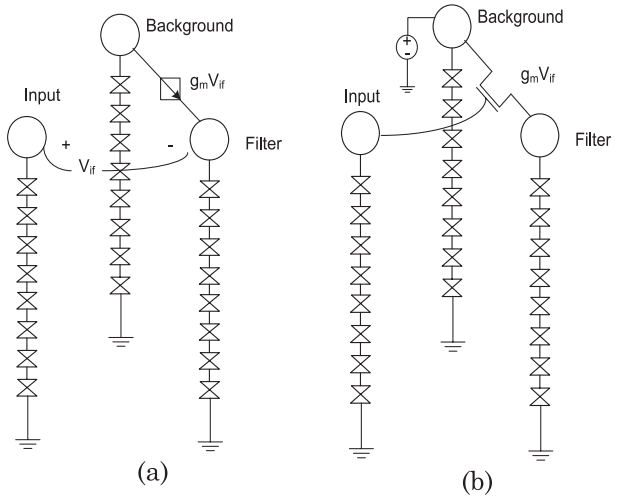

Fig. 10. Circuit configurations for color extraction: (a) using voltage-controlled current source; (b) using MOSFET.

between three cells is depicted as shown in Figure 10. However, if we want to represent the relationship with template methods, the feedback and feed-forward template can be represented as

$$a = \begin{pmatrix} 0 & m & 0 \\ 0 & 0 & 0 \\ 0 & 0 & 0 \end{pmatrix}, \quad b = \begin{pmatrix} 0 & 0 & 0 \\ n & 0 & 0 \\ 0 & 0 & 0 \end{pmatrix}.$$

The relationship between the inputs to outputs is represented as n, and the relationship between the background and output as m. From these templates, we expect the input image affects the conductance between the background output and the output image. The values of m, n are decided according to the devices for implementation.

The circuits shown in Figure 10 are designed to extract the color in the array of the multi-peak RTD structure. Figure 10(a) is the circuit which uses a voltage-controlled current source for color extraction. The input in Figure 10(a) is the RGB color value of the image to be processed. The background color after the color image processing is determined by the background cell value. Also, the filtering cell value is the color value of the image to be extracted.

In Figure 10(a), the change of the voltage in the filtering cell can be obtained by

$$C\frac{dV_{filter}}{dt} = -J(V_{filter}) + g_m V_{if}, \tag{22}$$

where g_m, V_{if}, and V_{filter} are conductance, voltage difference between the filtering cell and input cell, and voltage in the filtering cell, respectively.

Two methods can be used to assign the initial state in Figure 10. One is to initialize the filtering cells with one color value. The other method is to initialize the filter cells with the input image color value. These two methods can be used in both of the circuits in Figure 10.

As shown in Figure 10(a), the circuit implementation with the voltage-controlled current source is described. In this circuit, the color extraction is possible using the principle that when V_{if} is greater than threshold voltage, the result is a current flow from the background cell to the filter cell. Figure 10(b) shows the circuit implementation with a MOSFET instead of the voltage-controlled current source. The feasibility of

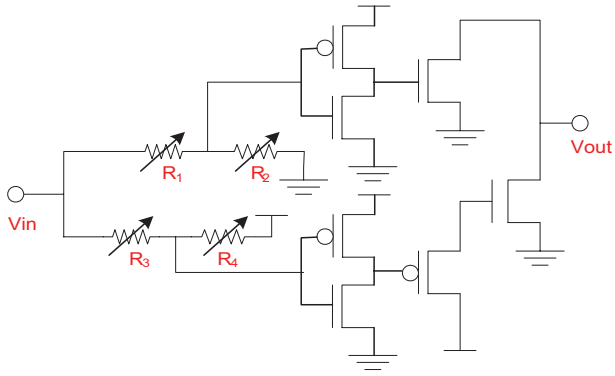

Fig. 11. A circuit configuration for any color extraction where Vout is initialized into Vin.

implementation with the MOSFET hybrid with III-V material is shown in patents and papers [Huang et al. 2008; Lee and Jeong 2004]. Even if it is not simple to fabricate this structure in these days, as the fabrication technology evolves, it will be getting easier in the future. In this article, we want to demonstrate the prototype of work which will be realized in the near future.

When the MOSFET is in the triode region, the change of the voltage in the filtering cell can be obtained by

$$C\frac{dV_{filter}}{dt} = -J(V_{filter}), + \mu_n C_{ox}\frac{W}{L}\left[(V_{if}-V_{TH})V_{bf}-\frac{1}{2}V_{bf}^2\right], \quad (23)$$

where $V_{if} - V_{bf} \leq V_{TH}$. In the saturation region, the change of the voltage in the filtering cell is given by

$$C\frac{dV_{filter}}{dt} = -J(V_{filter}), + \frac{1}{2}\mu_n C_{ox}\frac{W}{L}(V_{if}-V_{TH})^2(1+\lambda V_{DS}), \quad (24)$$

where $V_{if} - V_{bf} > V_{TH}$ and λ is the channel length modulation which is an empirical constant parameter.

The circuits in Figure 10(a) and (b) are limited in terms of the number of colors that can be extracted because the current controllers with the critical voltage allow only the extraction of the highest or lowest color value. Therefore, we suggest an advanced circuit which can extract any color in the image as shown in Figure 11. The color to be extracted is controlled by changing the four resistor values. The output voltage is given as follows.

$$V_{out} = V_{in}\begin{cases} V_{in}\cdot\dfrac{R_2}{R_1+R_2} > \dfrac{V_{DD}}{2} or \\ \dfrac{R_3}{R_3+R_4}V_{DD}+\dfrac{R_4}{R_3+R_4}V_{in} < \dfrac{V_{DD}}{2} \end{cases}$$

$$V_{out} = 0\begin{cases} V_{in}\cdot\dfrac{R_2}{R_1+R_2} < \dfrac{V_{DD}}{2} or \\ \dfrac{R_3}{R_3+R_4}V_{DD}+\dfrac{R_4}{R_3+R_4}V_{in} > \dfrac{V_{DD}}{2} \end{cases} \quad (25)$$

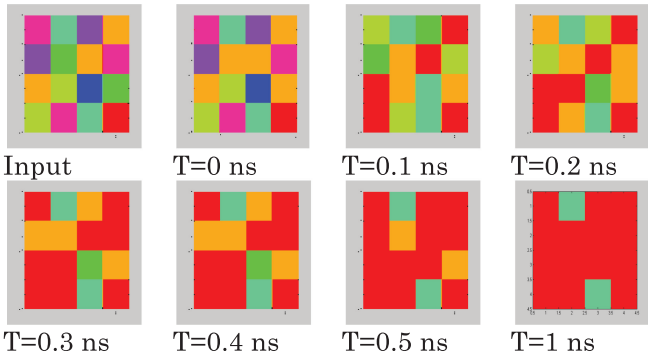

Fig. 12. Cyan color extraction of 4 × 4 pixel image using the circuit shown in Figure 11.

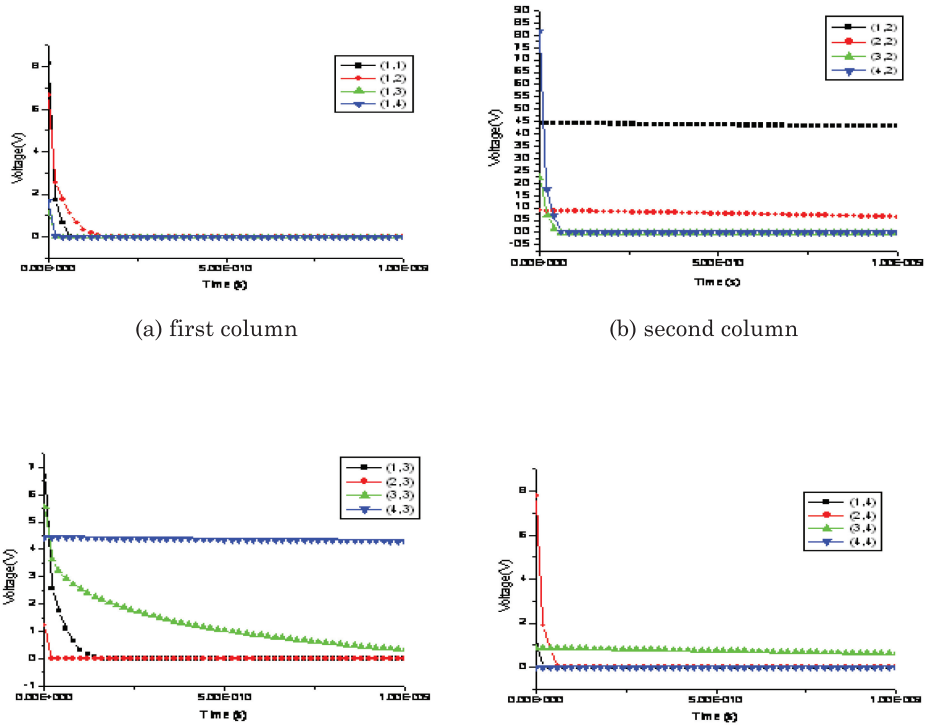

(a) first column (b) second column

(c) third column (d) fourth column

Fig. 13. HSPICE simulation results divided into columns with time from 0 ns to 1 ns.

Using the circuit in Figure 11, red color extraction of the 4 × 4 image is shown for time from 0 ns to 1 ns in Figure 12. The HSPICE simulation results with time are shown in Figure 13. The HSPICE simulation result of the changes of the color values confirms the final output image in Figure 12.

In Table II, comparisons in the performance and property of the image functions are described. The image processor shows better performance in the functions of the quantization and smoothing than color extraction. This originates from the devices for the function implementation. Since the conventional CMOS was used for the color extraction, the performance was dominated by the CMOS. However, this degradation

Table II. Comparison of Properties of Image Functions

Para-meters	Quantization	Smoothing	Color extraction	Color extraction
	(50×50)	(50×50)	(Figure 8(b)) (4×4)	(50×50)
Delay (worst case)	0.13 ns	0.6 ns	0.3 ns (w/o interconnect delay)	1.3 ns (w/o interconnect delay)
Power (worst case)	10 nW	10 nW	0.038 mW	0.015 W
Power-Delay Product	1.3×10^{-18} J	6×10^{-18} J	1.14×10^{-14} J	1.95×10^{-11} J
Resistor	250 MΩ	50 MΩ	NA	NA
Area	$\sim 50 \times 50$ (nm)^2	$\sim 50 \times 50$ (nm)^2	~ 2 (um)^2	~ 30 (um)^2

Table III. Operational Specifications for Different Processors

Parameters	DM 642	C641×	C6711	C55×
Frequency (MHz)	$400 \sim 600$	$500 \sim 600$	150	$144 \sim 200$
Power	$1 \sim 1.7$	$0.64 \sim 1.04$	1.1	$0.065 \sim 0.16$
CPI	$1.67 \sim 2.5$	$1.67 \sim 2$	6.7	$2.5 \sim 6.94$

Table IV. Performance Comparison among Different Processors for Smoothing Function (500×500 pixels)

Parameters	DM 642	C641×	C6711	C55×	Suggested processor
Smoothing (instructions)	$20 \times (1.67 \sim 2.5)$	$20 \times (1.67 \sim 2)$	$20 \times (6.7)$	$20 \times (2.5 \sim 6.94)$	1(*)
Smoothing (ns)	$55.6 \sim 125$	$66.8 \sim 80$	893	$250 \sim 964$	0.6
Power (W)	$1 \sim 1.7$	$0.64 \sim 1.04$	1.1	$0.065 \sim 0.16$	1×10^{-6}
Power-delay product (nJ)	~ 212.5	~ 83.2	982.3	~ 154	6×10^{-7}
Area (μm^2)	$\sim 25 \times 10^6$	$\sim 25 \times 10^6$	$\sim 25 \times 10^6$	$\sim 25 \times 10^6$	25×10

(*) The MPRTD processor data is based on HSPICE simulation as opposed to actual fabrication data of commercial microprocessors.

can be overcome by using nanoelectronic devices. This will be the focus of our further study.

7. COMPARISON WITH DSP CHIPS

In Table III, the performance comparison among commercial DSPs is described [Texas Instruments 2013a, 2013b, 2013c, 2013d, 2013e]. The operating frequencies range from 150 to 600 MHz. In the relationship between IPC and power dissipation, the power dissipation is reversely proportional to the IPC because the more processing instructions per clock cycles, the more the power dissipation.

In Table IV, the processing time and power dissipation comparison among different DSPs for the smoothing function is demonstrated. Based on Texas Instruments [2013e], the smoothing function requires around 20 instructions per pixel for averaging the neighboring pixel values and divided by the number of pixels. The processing time is calculated considering the CPI and frequency of the DSPs. The result shows that the DSPs are slower than the suggested image processor by 2 to 4 orders of magnitude. However, since we did not include interconnect delay and I/O delay for the suggested image processor, the realistic speed of the suggested image processor will be degraded by several nanoseconds, while the energy dissipation of the MPRTD-based processor is expected to be a few orders of magnitude lower than the DSPs' power consumption. Also, the area overhead of DSPs is bigger than the suggested processor by 5 orders of magnitude. Even if we consider the speed degradation by the interconnect delay, I/O delay, and area overhead of the I/O pad, the suggested image processor shows better performance than DSPs by a considerable margin.

Implementing parallel processing with the conventional DSPs, one can reduce the processing time comparable to the MPRTD image processor. However, this will increase

the power dissipation dramatically so that the implementation will become unrealistic. For instance, if we use 1000 DSPs for the parallel processing, the power dissipation will be around 1 KW. Therefore, this implementation will not be a promising approach to reduce the processing time. Therefore, under the tight energy and Silicon area budget, the MPRTD-based image processor will provide far superior performance than existing digital computers.

Using the structure with the single RTD plate as discussed in Roychowdhury et al. [1996] and Karahaliloglu and Balkir [2002] cannot process the color image algorithm such as the functions shown Table II as it has two states by itself. To process the color image algorithm, the structure needs to be changed by adding heavy interconnection between the cells. In this way, the gain of the compact size of the structure will disappear.

8. STABILITY

We must ensure that the networks of MPRTDs stabilize when an image function is performed by changing the programmable interconnects between the MPRTDs. To examine the stability of the nonlinear dynamic system describing the color image processor architecture, the classical Lyapunov theorem will be applied here. We consider an array of $M \times N$ MPRTD cells, where the cell on the ith row and jth column is denoted by $C(i,j)$. The output of the MPRTD on the ith row and jth column is represented by V_{ij}. We can then define the Lyapunov function, $E(t)$, of the MPRTD image processor by Eq. (26).

$$\begin{aligned} E(t) \;=\; & -\frac{1}{2}\sum_{n,m}\sum_{k,l} A(n,m;k,l)\cdot F_{n,m}(t)\cdot F_{k,l}(t) \\ & +\frac{1}{R(V_{n,m})}\sum_{n,m}\int_0^{F_{n,m}} G^{-1}(F_{n,m})dF_{n,m} \\ & -\sum_{n,m}\sum_{k,l} B(n,m;k,l)\cdot F_{n,m}(t)\cdot U_{k,l}(t) \\ & -\sum_{n,m} I_{n,m}F_{n,m}(t) \end{aligned} \tag{26}$$

Here $U_{k,l}(t)$, $F_{n,m}(t)$, and G are feed-forward inputs, outputs from neighboring cells, and the relationship between the neighboring cell output and the target cell output. The stability of the image processor can be established by the following two theorems that claim the Lyapunov energy function is both bounded for a given power supply for the MPRTD image processor and the energy function monotonically reduces to a minimum value.

THEOREM 1. *The Lyapunov function, $E(t)$, of the multi-peak RTD-based color image processor is bounded by E_{max} when a supplied voltage source is bounded.*

PROOF. If the supplied voltage source is bounded, $V_{n,m}$, $F_{k,l}$, $V_{k,l}$, and $U_{k,l}$ are bounded. If $V_{n,m}$ is bounded, the differential resistance which is the function of $V_{n,m}$ is also bounded. The current flow between the neighboring cells and the target cell which is defined as $A(i,j;k,l)$ and $B(i,j;k,l)$ is bounded as the supplied voltage source is bounded. Considering a bounded external current source, $E(t)$ is bounded. □

THEOREM 2. *The differential of the Lyapunov function, E(t), of the multi-peak-based color image processor is less than or equal to zero in the region where $dF_{n,m}/dV_{n,m} \geq 0$,*

that is

$$\frac{dE(t)}{dt} \leq 0 \quad where \quad \frac{dF_{n,m}}{dV_{n,m}} \geq 0. \tag{27}$$

PROOF. From Eq. (26), the differential of $E(t)$ with respect to time t can be described by

$$\begin{aligned}
\frac{dE(t)}{dt} &= -\sum_{n,m}\sum_{k,l} A(n,m;k,l)\frac{dF_{n,m}}{dV_{n,m}} \cdot \frac{dV_{n,m}}{dt} \cdot F_{k,l}(t) \\
&\quad + \frac{1}{R(V_{n,m})}\sum_{n,m}\frac{dF_{n,m}}{dV_{n,m}} \cdot \frac{dV_{n,m}}{dt} \cdot G^{-1}(F_{n,m}) \\
&\quad - \sum_{n,m}\sum_{k,l} B(n,m;k,l)\frac{dF_{n,m}}{dV_{n,m}} \cdot \frac{dV_{n,m}}{dt} \cdot U_{k,l}(t) \\
&\quad - \sum_{n,m} I_{n,m} \cdot \frac{dF_{n,m}}{dV_{n,m}} \cdot \frac{dV_{n,m}}{dt} \\
&= -\sum_{n,m}\frac{dF_{n,m}}{dV_{n,m}} \cdot \frac{dV_{n,m}}{dt}\left(\sum_{k,l} A(n,m;k,l) \cdot F_{k,l}(t) - \frac{G^{-1}(F_{n,m})}{R(V_{n,m})}\right. \\
&\quad \left. + \sum_{k,l} B(n,m;k,l) \cdot U_{k,l}(t) + I_{n,m}\right) \\
&= -\sum_{n,m}\frac{dF_{n,m}}{dV_{n,m}} \cdot \left[\frac{dV_{n,m}}{dt}\right]^2 \cdot C. \quad \square
\end{aligned} \tag{28}$$

Since we can assume C is positive in physical meaning, the polarity of $E(t)/dt$ depends on $dF_{n,m}/dV_{n,m}$. From this theorem, the multi-peak RTD-based color image processor is stable in a limited region where $dF_{n,m}/dV_{n,m} \geq 0$. The differential of $F_{n,m}$ with respect to $V_{n,m}$ is positive when the differential resistance of the multi-peak RTD is positive. When the functions of the color image processor are the quantization or smoothing function, the template A is changed and has all positive values. In the case of color extraction, the template A has positive values which are the variable with respect to the $F_{k,l}$ and template B also has positive values which are the variable with respect to the $U_{k,l}$. The changed template A and B do not affect the stability of the image processor. Based on Eq. (28), the multi-peak RTD-based color image processor is stable regardless of the functions of the image processor.

9. CONCLUSION

In this article, we have introduced a new architecture to process color images by using a spatially distributed array of multi-peak RTDs. We have demonstrated through simulation various color image processing functions such as the quantization, smoothing, and color extraction by programming the interconnecting patterns (synapses) between the MPRTDs which act as neurons. We implemented a quantization function and smoothing function through changing the conductance value between the MPRTDs. In the case of the color extraction function, we suggested three different methods to extract the selected colors. We demonstrate the HSPICE simulation results of these functions. Based on the simulation, we demonstrate that 130 ps processing time is required for quantization, 600 ps for smoothing, and 1.3 ns for color extraction. Evidently, these performance data affirm that the MPRTD-based color image processor provides faster

processing speed and lower power dissipation than the conventional Digital Signal Processors (DSPs) as shown in Table IV.

REFERENCES

ARENA, P., FORTUNA, L., AND OCCHIPINTI, L. 2002. A cnn algorithm for real time analysis of dna microarrays. *IEEE Trans. Circ. Syst. I: Fundam. Theory Appl. 49*, 3, 335–340.

CHUA, L. O. AND YANG, L. 1988. Cellular neural networks: Applications. *IEEE Trans. Circ. Syst. 35*, 1273–1290.

CHANG, L. L., ESAKI, L., AND TSU, R. 1974. Resonant tunneling diode in semiconductor double barriers. *Appl. Phys. Lett. 24*, 593–595.

DING, L. AND MAZUMDER, P. 2004. Noise- tolerant quantum mos circuits using resonant tunneling devices. *IEEE Trans. Nanotechnol. 3*, 134–146.

HADDAD, G. I. AND MAZUMDER, P. 1997. Tunneling devices and their applications in high-functionality/speed digital circuits. *J. Solid State Electron. 41*, 10, 1515–1524.

HÄNGGI, M. AND CHUA, L. O. 2001. Cellular neural networks based on resonant tunnelling diodes. *Int. J. Circ. Theory Appl. 29*, 5, 487–504.

HUANG, W., LI, Z., CHOW, T. P., NIIYAMA, Y., NOMURA, T., AND YOSHIDA, S. 2008. Enhancement-mode gan hybrid mos-hemts with ron, sp of 20 mω-cm2. In *Proceedings of the 20th International Symposium on Power Semiconductor Devices and IC's (ISPSD'08).* 295–298.

KARAHALILOGLU, K. AND BALKIR, S. 2002. Image processing with quantum dot nanostructures. In *Proceedings of the International Symposium on Circuits and Systems*. Vol. 5. 217–220.

KARAHALILOGLU, K., BALKIR, S., PRAMANIK, S., AND BANDYOPADHYAY, S. 2003. A quantum dot image processor. *IEEE Trans. Electron. Dev. 50*, 7.

LEE, B.-H. AND JEONG, Y.-H. 2004. A novel set/mosfet hybrid static memory cell design. *IEEE Trans. Nanotechnol. 3,* 3, 377–382.

LEE, W. H. AND MAZUMDER, P. 2008. Motion detection by quantum dots based velocity tuned filter. *IEEE Trans. Nanotechnol. 7,* 3, 355–362.

MAZUMDER, P., KULKARNI, S., HADDAD, G. I., AND SUN, J. P. 1998. Digital applications of quantum tunneling devices. *Proc. IEEE* 664–688.

PRATT, W. 2001. *Digital Image Processing* 3rd Ed. Wiley.

ROYCHOWDHURY, V. P., JANES, D. B., AND BANDYOPADHYAY, S. 1996. Collective computational activity in self-assembled arrays of quantum dots: A novel neuromorphic architecture for nanoelectronics. *IEEE Trans. Electron. Dev. 43*, 10, 1688–1699.

SEABAUGH, A. AND MAZUMDER, P. 1999. Quantum devices and their applications. *Proc. IEEE 87*, 4, 535–536.

SEABAUGH, A. C., KAO, Y. C., AND YUAN, H. T. 1992. Nine-state resonant tunneling diode memory. *IEEE Electron. Dev. Lett.13*, 9, 479-481.

SUN, J. P., HADDAD, G. I., MAZUMDER, P., AND SCHULMAN, J. N. 1998. Resonant tunneling diodes: Models and properties. *Proc. IEEE 86,* 641–660.

TETZLAFF, R., KUNZ, R., AMES, C., AND WOLF, D. 1999. Analysis of brain electrical activity in epilepsy with cellular neural networks (cnn). In *Proceedings of the European Conference on Circuit Theory and Design.*

TEXAS INSTRUMENTS. 2013a. TMS320C6711 dsk. http://focus.ti.com/docs/toolsw/folders/print/tmds320006711.html.

TEXAS INSTRUMENTS. 2013b. TMS320DM642 product folder. http://focus.ti.com/docs/toolsw/folders/print/tmds320dm642.html.

TEXAS INSTRUMENTS. 2013c. TMS320DM642 power consumption. http://focus.ti.com/lit/an/spra962a/spra962a.pdf.

TEXAS INSTRUMENTS. 2013d. TMS320C6416 product folder. http://focus.ti.com/docs/prod/folders/print/tms320c6416.html.

TEXAS INSTRUMENTS. 2013e. TMS320C6416 power consumption. http://focus.ti.com/lit/an/spra811c/spra811c.pdf. http://focus.ti.com/dsp/docs/dsphome.tsp?sectionId=46&DCMP=TIHeaderTracking&HQS=Other+OT+hdr_p_dsp.

WAHO, T., CHEN, K. J., AND YAMAMOTO, M. 1998. Resonant-tunneling diode and hemt logic circuits with multiple thresholds and multilevel output. *IEEE J. Solid-State Circ. 33*, 2.

WANG, L., DE GYVEZ, J. P., AND SANCHEZ-SINENCIO, E. 1998. Time multiplexed color image processing based on a cnn with cellstate outputs. *IEEE Trans. VLSI Syst. 6*, 2, 314–322.

Received January 2010; revised March 2012; accepted May 2012